JGR Space Physics

RESEARCH ARTICLE
10.1029/2020JA027922

The Evolution of Long-Duration Cusp Spot Emission During Lobe Reconnection With Respect to Field-Aligned Currents

Jennifer A. Carter[1], Stephen E. Milan[1], Alexandra R. Fogg[1], Harneet Sangha[1], Mark Lester[1], Larry J. Paxton[2], and Brian J. Anderson[2]

[1]Department of Physics and Astronomy, University of Leicester, Leicester, UK, [2]Applied Physics Laboratory, John Hopkins University, Laurel, MD, USA

Key Points:

- Extreme IMF-By causes distortions of polar cap aurora and field-aligned currents
- The study of cusp spots provides a method to remotely investigate reconnection sites at the distant magnetopause
- A cusp spot is found in the sunward flow region between cells of FAC under persistent northward IMF

Correspondence to:
J. A. Carter,
jac48@leicester.ac.uk

Citation:
Carter, J. A., Milan, S. E., Fogg, A. R., Sangha, H., Lester, M., Paxton, L. J., & Anderson, B. J. (2020). The evolution of long-duration cusp spot emission during lobe reconnection with respect to field-aligned currents. *Journal of Geophysical Research: Space Physics*, *125*, e2020JA027922. https://doi.org/10.1029/2020JA027922

Received 18 FEB 2020
Accepted 4 JUN 2020
Accepted article online 10 JUN 2020

Abstract We track a remarkably bright and persistent auroral cusp spot emission in the high-latitude Northern Hemisphere polar cap, well inside the main auroral oval, for approximately 11 hr on 16 and 17 June 2012. The auroral emissions are presented in both the Lyman-α and Lyman-Birge-Hopfield bands, as observed by the Special Sensor Ultraviolet Spectrographic Imager on board two of the Defense Meteorological Satellite Programme spacecraft, and supported by detections of precipitating particles by the same spacecraft. The auroral observations are accompanied by patterns of field aligned currents, obtained from the Active Magnetosphere and Planetary Electrodynamics Response Experiment, along with ionospheric convection patterns from the Super Dual Auroral Radar Network. These data provide unprecedented coverage of a cusp spot, unusually seen in both electron and proton aurora.
The location and movement of the auroral emissions, current systems, and ionospheric convection patterns are extremely distorted under the northward to *Y*-component-dominated interplanetary magnetic field. The cusp spot emission region is associated with the sunward flow region of the ionosphere. Ion dispersion signatures are detected on traversal of the region of brightest proton auroral emissions. Proton-excited Lyman-α emissions are most evident following impulses of high solar wind density. The auroral emissions, field-aligned current patterns, and ionospheric convection are consistent with a model of a compressed magnetosphere under strongly northward interplanetary magnetic field, following an impact of an Interplanetary Coronal Mass Ejection and associated magnetic cloud at the magnetopause, inducing high-latitude lobe reconnection that progresses increasingly tailward during the presented interval.

1. Introduction

The investigation of localized auroral emissions, found inside the main auroral oval, provides a method to remotely sense various phenomena occurring in the wider magnetosphere. For example, under prevailing northward interplanetary magnetic field (IMF) conditions, an auroral "cusp spot" may be observed, as shown by Milan et al. (2000) and Frey et al. (2002). This emission is found poleward of the main auroral oval and maps to open magnetic field lines that will be undergoing high-latitude lobe reconnection at the magnetopause (Sandholt et al., 1998). The auroral emissions result from direct precipitation of particles from the magnetosheath into the polar cap (Escoubet et al., 2013; Fuselier et al., 2003; Milan et al., 2000). The location of the cusp spot has been shown to move in response to the east-west (B_Y) orientation of the IMF; for $B_Y < 0$ nT and $B_Y > 0$ nT in the Northern Hemisphere, it is located in the prenoon and postnoon sectors, respectively (Frey et al., 2003).

Bryant et al. (2013) identified two types of proton-induced auroral emissions within the Northern Hemisphere polar cap, characterizing these emissions by their proximity to the main auroral oval. Their "polar cap spots" occurred during northward IMF and were found poleward of the main auroral oval. They attribute these polar cap spots to interactions of the magnetosphere with radially orientated IMF (primarily negative B_X component), at large IMF azimuth angles, so that reconnection occurs in the high-latitude lobes on open field lines in the Northern Hemisphere. The polar cap spots are weaker in emission intensity, and with less spatial extension, than the other class of auroral emissions, namely, "auroral oval

spots," which were shown to occur during either northward or southward IMF. Bryant et al. (2013) reported that the intensity of the aurora oval spots was proportional to the solar wind density, and therefore the number of precipitating particles.

Other phenomena associated with northward IMF include High Latitude Detached Arcs (HiLDAs). These have been associated with the upward NBZ field-aligned current (FAC) cell produced by lobe reconnection (Frey, 2007; Frey et al., 2003, 2004; Korth et al., 2005, and references therein). The NBZ current cells are found poleward of the main Region 1, Region 2 current system, as observed by Iijima et al. (1984), Araki et al. (1984) and Vennerstrøm et al. (2002), and consist of a pair of upward and downward FACs either side of the noon-midnight meridian. HiLDAs are observed in the summer hemisphere (Carter et al., 2018) and are therefore linked to the increased conductivity, through photoionization, of the sunlit hemisphere.

In this paper we present a detailed and comprehensive study of a Northern Hemisphere cusp spot over an 11 hr period. We accompany the auroral images with supporting data sets of ionospheric convection velocity, distributions of FACs, and particle precipitation for both ions and electrons. There remains controversy in the community regarding the physical mechanisms resulting in various high-latitude, polar cap phenomena, particularly under northward IMF conditions, such as differences between HiLDAs and cusp spots, and this paper aims to resolve this issue. This data set provides an unprecedented opportunity to examine the cusp spot, with respect to both the distribution of FACs across the polar cap and ionospheric convection. Moreover, this allows us to identify the extreme distortion of the NBZ FAC and auroral morphology during periods of large IMF B_Y. This paper is organized as follows. In section 2 we briefly describe our data sets. In section 3 we present a selection of images of auroral emissions and FAC distributions, with accompanying radar data and precipitating particle spectrograms from the interval when the cusp spot was observable. We present a profile of the accompanying IMF and solar wind conditions for the interval. In section 4 we discuss our results with respect to the movement of the cusp spot in relation to high-latitude lobe reconnection. We conclude in section 5.

2. Data

Images of auroral emissions are obtained by the Special Sensor Ultraviolet Spectrographic Imager (SSUSI) instrument (Paxton & Zhang, 2016; Paxton et al., 1992) for 16 and 17 June 2012. This instrument is flown on the F16, F17, and F18 Air Force Defense Meteorological Satellite Program (DMSP) spacecraft. The SSUSI scanning image spectrograph (SIS) photon-counting detectors are sensitive to ultraviolet wavelengths at five spectral wavelengths or bands. In this work we use SSUSI radiance data in the Lyman-Birge-Hopfield long (LBHl) band (165–180 nm) and in the Lyman-α (121.6 nm) channel. We present data from F16 and F18 only. We exclude data from the F17 instrument, as these have suffered from a lack of response in the Lymna-α and atomic oxygen channels, likely due to an issue with the construction of the grating. Images of polar auroral emissions are built up in swathes over a time period of approximately 20 min, as each DMSP spacecraft moves along their polar Sun-synchronous orbital path (Paxton et al., 2018). The images available in the SSUSI public archive have been corrected for dayglow, and radiances are rectified to pierce-point equivalent nadir pointing by the SSUSI project team (Liou et al., 2011; Paxton et al., 2017; Strickland et al., 1995, 2004; Zhang & Paxton, 2008). The high-latitude polar cap of each hemisphere is observed approximately every 1.5 hr by an individual spacecraft. It would have been beneficial to include Southern Hemisphere SSUSI data in our characterization of the cusp spot for tests of interhemispheric conjugacy, but due to the local solar time of the ascending node and the inclination of the orbit at these particular UTs, only the nightside portion of the polar cap is visible, and therefore, the Southern Hemisphere data have been omitted from this study.

We also present data from the DMSP F16 and F18 Special Sensor J (SSJ/5) instruments, which monitor both electron and ion particle precipitation (Redmon et al., 2017), in 20 energy channels between 30 eV and 30 keV.

To accompany the auroral emission images, distributions of FACs are obtained from the Active Magnetosphere and Planetary Electrodynamics Response Experiment (AMPERE), acquired from the measurements of perturbations in the engineering magnetometers onboard the Iridium telecommunication satellite constellation (Anderson et al., 2000; Waters et al., 2001). These distributions are constructed by averaging the component FAC maps, available at 2-min resolution, that occur during each

DMSP/SSUSI polar cap pass. The inferred current densities provided by AMPERE are given in grids of 1 hr of MLT by 1° of colatitude.

We make use of ionospheric convection velocity data, available at 2-min resolution, from the Super Dual Auroral Radar Network (SuperDARN, e.g., Chisham et al., 2007; Greenwald et al., 1995; Nishitani et al., 2019). All available radar data have been processed using the SuperDARN software *FitACF*, Version 3.0, using the Radar Software Toolkit 4.2 (SuperDARN Data Analysis Working Group et al., 2018), and assimilated using the map potential technique (Ruohoniemi & Baker, 1998). A new method to refine the latitude selection of the Heppnard-Maynard boundary that defines the lower limit in latitude of ionospheric convection has been employed, by using AMPERE data to derive a proxy for the boundary between the Regions 1 and 2 currents (Fogg et al., 2020). Vectors with speeds of less than 100 m s^{-1} are not considered in our analysis here.

Solar wind data examined in this paper were obtained from the OMNI database (King & Papitashvili, 2005), which have been adjusted in time for propagation to the dayside bow shock.

3. Results

In Figure 1 we plot the IMF and solar wind conditions, geomagnetic indices, plus total currents from AMPERE and mean radiances from SSUSI, encompassing the time interval of the observable cusp spot. In Figure 1a, we plot the IMF B_Y and B_Z components, plus the magnitude of the IMF, in pink, green, and gray. The IMF is northward (positive B_Z), except for a few short excursions below 0 nT before 23 hr UT, before turning definitely southward at ~05 hr UT. We observe a rotation in the IMF B_Y and B_Z components during this interval. The B_Y component changes from near zero, to positive, through to negative and back to positive again, and it remains positive for the remainder of the interval. The B_Z component skims zero, rises to positive, and then back to near zero, before returning to highly positive, or northward, until the southward turning at ~05 hr UT. This is evidence of a passing interplanetary coronal mass ejection (ICME) with an embedded magnetic cloud structure. In Figure 1b, we plot the solar wind density (gray), solar wind speed (sky blue), and solar wind pressure (brown). The solar wind speed varies smoothly throughout, and therefore, variations in the solar wind pressure are driven by the fluctuations in the solar wind density. In Figure 1c we plot the upper and lower auroral electrojet indices AU and AL. These indices show some activity between 21 and 23 hr UT, followed by prolonged bays from shortly before 03 hr UT. In Figure 1d we plot, in orange, the derived magnetopause stand-off distance at the subsolar point in this panel, calculated using the model of Shue and Song (2002). This derived magnetopause distance is dependent on the instantaneous solar wind dynamic pressure and IMF B_Z component. Under this model, the magnetopause would be considerably compressed from its nominal value of 10 R_E, between approximately 20 and 03 hr UT. This compression occurs even under strongly northward IMF conditions and is driven by the large solar wind pressures as shown in Figure 1b. We also plot the SYM-H index, in gray, which measures deviations in horizontal components of the geomagnetic field and senses variations in the ring current. SYM-H is large and very positive throughout this entire period, indicating the absence of any geomagnetic storm at this time but showing the extreme effect of the compressed magnetosphere on ground magnetic perturbations. In Figure 1e we plot the total upward and downward current, given in MA and plotted in red and blue, respectively, for a dayside polar cap region limited in spatial extent between 0° and 12° colatitude and between 6 and 18 hr MLT. These total currents were calculated from AMPERE current densities, using an assumed altitude of 110 km, at 2-min resolution. Following a more relaxed threshold as recommended by Clausen et al. (2012), current densities with values equal or greater than 0.1 μA m^{-2} absolute current magnitude were included. In Figure 1f we plot the mean radiances as measured by SSUSI for the LBHl (purple) and Lyman-α (sky blue) emissions. The mean radiances taken from the same spatial region as that of Figure 1e are marked by the empty rectangles, whereas the mean emissions for each whole SSUSI image are marked by filled rectangles. An increase in the mean emissions in the dayside polar cap, particularly for the LBHl emissions, is observed from 22 hr UT and continues to be elevated for the remainder of the interval. After 07 hr UT (not shown), there is no visible auroral cusp spot inside the polar cap, when we determine this interval to end. The Lyman-α emissions in the polar cap region are much weaker and are not raised above that of the main auroral oval, only showing significant enhancements at 22:09 and 01:36 hr UT, at times approximately coincident with increases in the solar wind density. In Figure 1g we

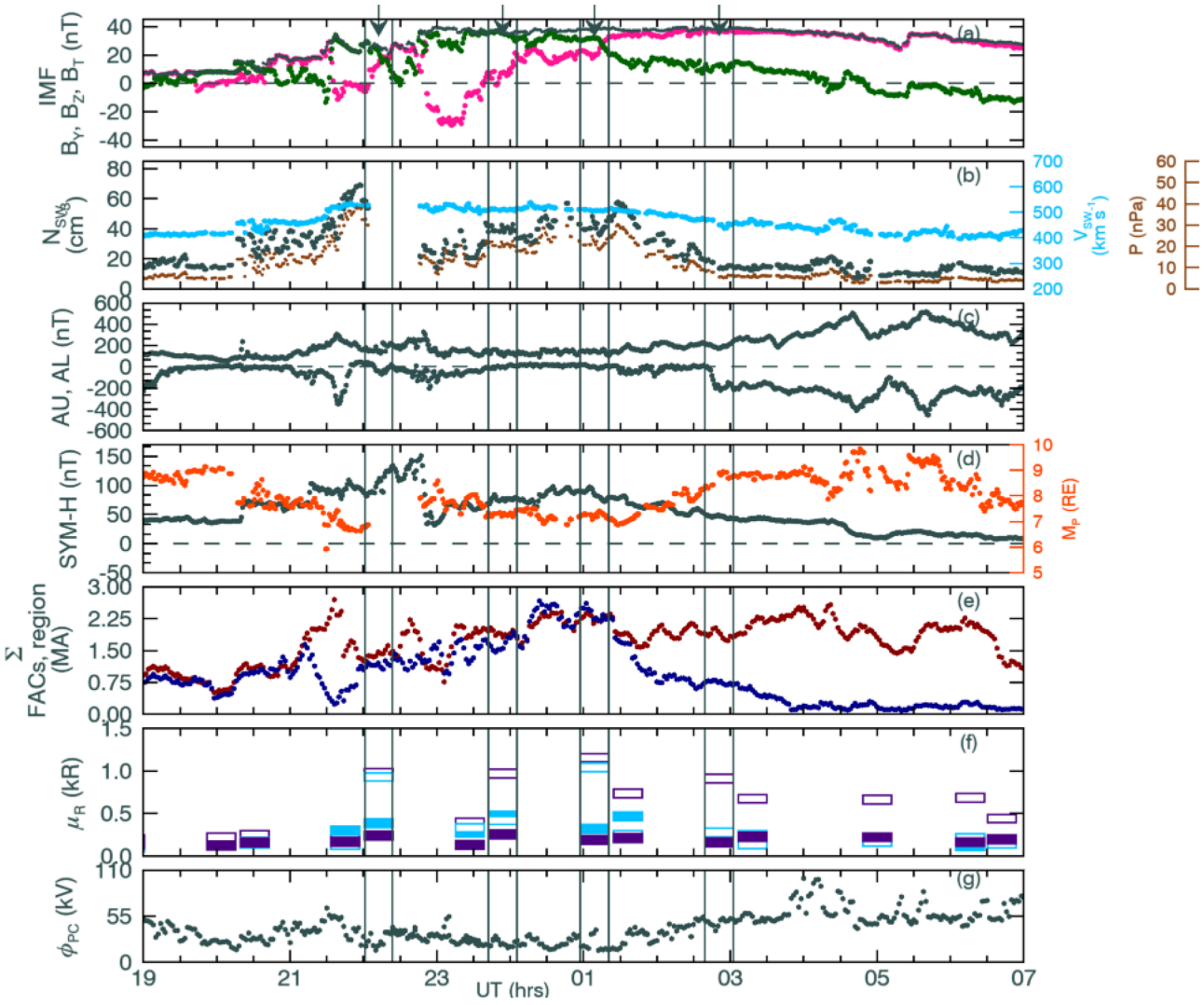

Figure 1. IMF (a) and solar conditions (b) during the appearance of the cusp spot, where IMF B_Y is in pink, B_Z is green, and B_T is in gray; solar wind density, speed, and flux are colored gray, blue, and brown, respectively. We also plot geomagnetic auroral indices (c) and SYM-H (gray), and Shue and Song (2002) modeled magnetopause location (orange, d). Dayside current amplitudes are shown in (e) where red is for upward and blue for downward current. Mean SSUSI-derived radiances are shown in (f), where purple and blue symbols are for LBH-long and Lyman-α radiances respectively, and where empty symbols are for the mean dayside polar cap SSUSI-image-derived radiances only, whereas filled symbols show mean values from the whole SSUSI image. The SuperDARN-derived cross polar cap potential (g) during our period of interest. Times are marked in UT (hr), and the time series runs from late 16 June 2012 into the first part of 17 June 2012. Arrows above the first panel indicate midtimes of the polar cap orbital passes presented in Figures 2–5, with vertical lines in gray marking the stop and start times of each pass. Each panel is described in detail in the text.

plot the cross polar cap potential, obtained from the SuperDARN plots described in section 2. The behavior of the cross polar cap potential follows the expected lack of dayside driving under northward IMF conditions. Increases in the cross polar cap potential are seen coincident with southward turnings of the IMF, particularly after ~04 hr UT.

An auroral cusp spot is weak, but visible in DMSP/SSUSI data from the Northern Hemisphere, beginning with the F18 satellite pass that starts at 20:21 hr UT on 16 June 2012. Although there is an F16 pass immediately prior to this F18 pass where the emission in the polar cap is nonzero, it is extremely weak and diffuse and is not spatially confined to a spot feature. This F16 pass prior to 20:21 hr UT does not observe the noon region of the polar cap at latitudes greater than 10° colatitude. The spot is then visible until the F18 pass that ends on 06:54 hr UT on 17 June 2012. In Figures 2–5, we plot selected DMSP, AMPERE, and SuperDARN data from this period, to illustrate the evolution and movement of the auroral cusp spot in the Northern Hemisphere over the varying solar wind conditions.

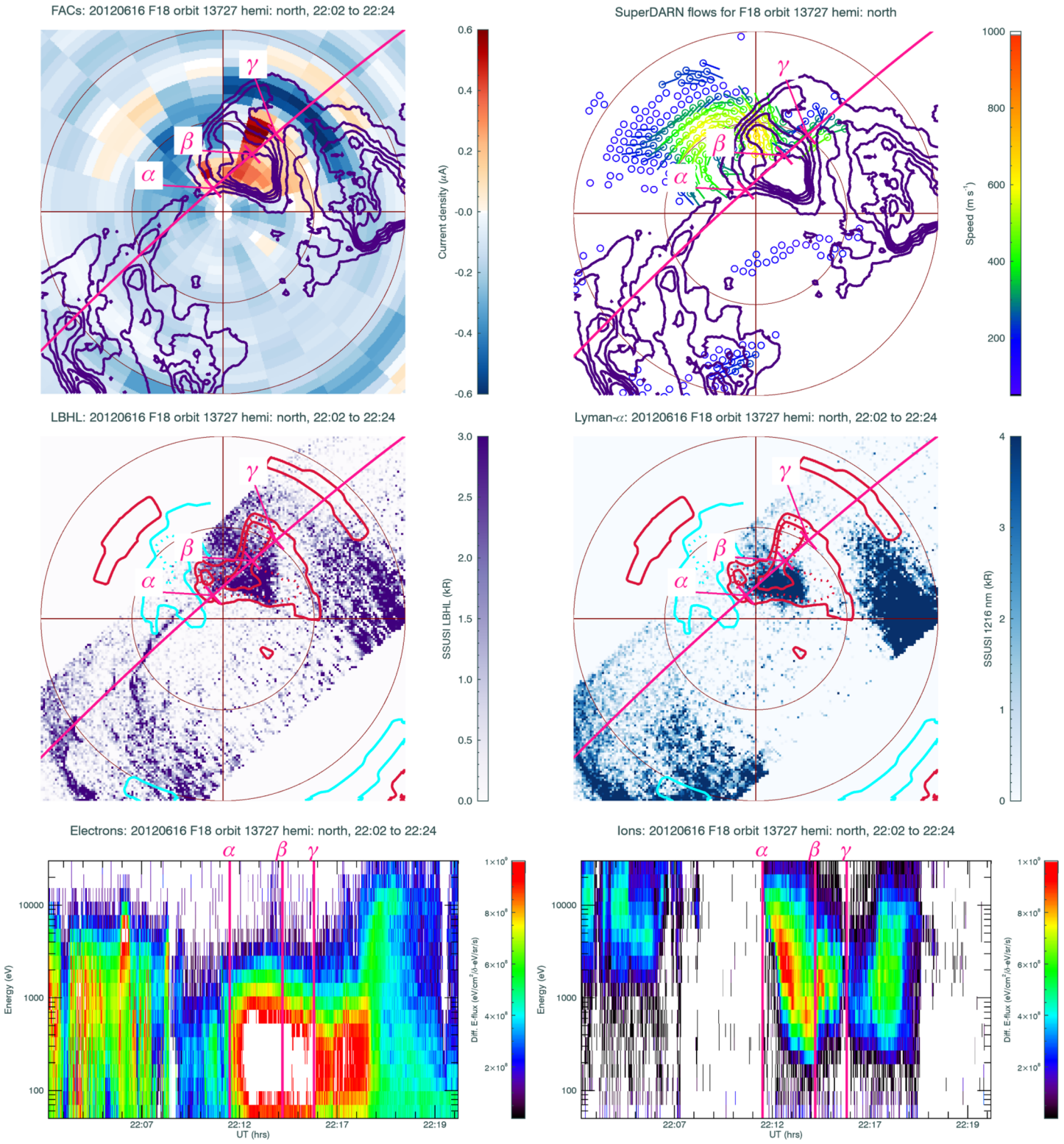

Figure 2. A selection of images relevant to DMSP F18 Orbit 13727. Top left: FAC distributions, with overlaid LBH-l contours (purple). Top right: ionospheric convection flows, color coded by speed, with LBH-l as before. Middle left and right: LBH-l then Lyman-α emissions with contours of upward and downward FAC, in red and blue, respectively. Bottom left and right: electron and ion spectrograms. In the top four panels, a satellite track is marked in dark pink. Labels on these panels, connected to points of interest on the satellite tracks via lines in pink, refer to the features marked on the spectrograms.

Each figure consists of six panels. The upper four images are plotted on a magnetic local time (MLT), magnetic colatitude grid, with 12 hr MLT to the top of each panel and 18 hr MLT to the left. DMSP satellite tracks are shown in pink. Annotations along these tracks, labeled by symbols, refer to features of interest that we discuss further in the text below.

The top left panel of each figure shows the distribution of AMPERE FAC densities averaged over the duration of the SSUSI Northern Hemisphere high-latitude pass, with red indicating upward currents and blue indicating downward currents. The top right panel shows SuperDARN ionospheric flows colored by speed, constructed from data in the 2-min interval closest to the midpoint of the orbital polar cap pass. The flows are shown as "flag poles," with the "flag" indicating the direction of flow. Speeds range from 100 m s^{-1} at the blue end of the color scale, to 1,000 m s^{-1}, which are colored red. The middle left panel contains an image of DMSP/SSUSI LBHl emissions, and the middle right panel contains an image of DMSP/SSUSI Lyman-α emissions with AMPERE contours.

On all of the image panels, concentric rings and lines in dark red indicate colatitudes at 10° and 20° colatitude and the noon-midnight and dawn-dusk meridians. Contours are plotted at 4-kV intervals, with the positive cell indicated by the dashed lines. Note that the color bars of the DMSP/SSUSI emissions have been scaled to highlight auroral features inside the polar cap region.

In the bottom left and right panels we plot DMSP SSJ/5 particle precipitation data as spectrograms for both electrons and ions, respectively, to accompany the auroral emissions in the preceding images. Vertical lines marked with labels refer to the same features as found on the satellite tracks in the preceding images. Panels are stamped with details of the date, DMSP satellite, orbit number, hemisphere, and time in hr UT of each SSUSI pass of the high-latitude polar cap where relevant.

For F18 Orbit Pass 13727, the auroral cusp spot emissions are bright for both LBHl and Lyman-α, as shown in the feature marked between α and β in Figure 2. A weak transpolar arc is seen in the LBHl emissions in the postdusk sector. Across noon, sunward flow vectors are seen, with a suggestion of an anticlockwise cell in the high-latitude postnoon sector. The satellite track bisects the cusp spot, moving from left to right in the images. High fluxes of both electrons and ions are seen between α and β, and between these times, an ion dispersion signature is seen. A second, but shorter and less energetic ion dispersion signature is observed between β and γ. The ion dispersion signature is indicative of high-latitude lobe reconnection, as established by Chisham et al. (2004, and references therein). During this DMSP pass, the IMF B_Y component becomes increasingly positive. This will move the lobe reconnection site eastward, as shown by the position of upward NBZ FAC cell slightly toward noon from a nominal IMF B_Y=0 position, seen in both Figure 2 first and second rows whereby the red upward cell begins to encroach into the postnoon sector. SuperDARN ionospheric flows, observed at a time mid-DMSP pass at 22:13 hr UT, are observed in the postnoon sector, in the region of the downward NBZ FAC cell. The solar wind density is extremely elevated immediately prior to this pass, as shown in Figure 1b. Just before this polar-cap pass, a negative excursion is seen in the AL index, as shown in Figure 1c, perhaps indicative of a small substorm that has been provoked by the arrival of the large pressure pulse just before 22 hr UT. Figure 1d shows that SYM-H is very large and positive during this pass, indicating a compression of the dayside magnetopause. The upward and downward polar cap FACs are of similar magnitude, as observed in Figure 1e.

We examine F18 Pass 13728 in Figure 3. By 23:43 hr UT the IMF B_Y component has returned to a small but positive value, and the IMF remains strongly northward. The NBZ FAC cells inside the polar cap have moved to a more symmetrical distribution about noon as compared to that in Figure 2. These high-latitude NBZ FACs have high current densities and are more apparent than the Regions 1 and 2 FACs, which are weakly observed at latitudes below ~78° latitude. The magnitudes of the NBZ current densities, as shown in Figure 1e, have increased. The brightest LBHl emissions are seen along the noon meridian and extend slightly into the night side of the polar cap. These brightest emissions are found in between the NBZ FAC cells, suggesting that they correspond to the sunward convection region. The Lyman-α emissions are brightest at the highest latitudes and fade quickly equatorward. The mean emissions are bright compared to the rest of the auroral oval, as shown in Figure 1f, particularly for the LBHl emissions. The satellite transects the cusp spot between δ and ϵ, when high fluxes are seen in both the electron and ion spectrograms. Two ion dispersion signatures can be seen in quick succession in the spectrograms, as the satellite track crosses

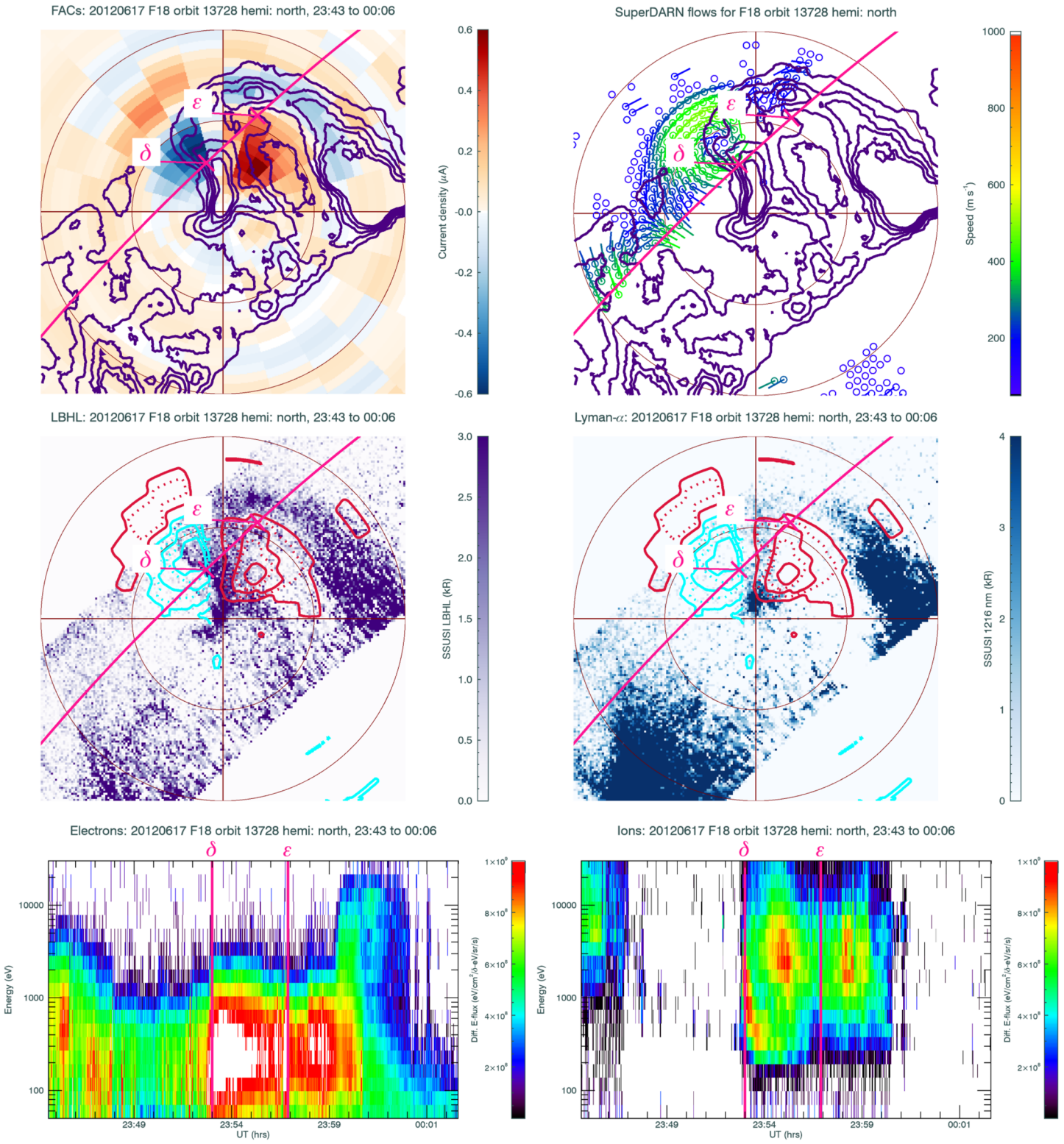

Figure 3. A selection of images relevant to DMSP F18 Orbit 13728. The format of the plots follows that of Figure 2.

the emission region between approximately 85° and 80° latitude. The ionospheric flows, observed at time mid-DMSP pass at 23:54 hr UT, here are again observed only in a spatially limited region and are colocated with the postnoon downward NBZ FAC cell. However, these flows are consistent with sunward flow

colocated with the cusp spot as suggested by the NBZ currents. During this pass, the solar wind density pulse seen during the previously presented pass has subsided, but the absolute values of these densities are still elevated above that of a nominal solar wind.

The cusp spot has moved to the postnoon sector by F16 Pass 44699, as shown in Figure 4. The IMF B_Y component has increased to a high positive value of approximately 30 nT and remains high for the rest of the time series. The IMF continues to be strongly northward. The positive high-latitude NBZ FAC cell dominates the polar cap spatially and is highly distorted and has moved from the dawn to the dusk side. The downward cell is pushed toward dusk. The magnitudes of the polar cap FACs are similar and large, at ~2.25 MA. Both LBHl and Lyman-α emissions are bright, and Figure 1f shows that the mean emissions inside the polar cap are much stronger than the rest of the polar cap emissions. The emissions are found at the eastern edge of the upward NBZ FAC cell and in the gap between the upward and downward cells, placing it in the region of sunward flows. Ionospheric flow vectors are seen distributed in various places at different locations within the polar cap, as shown in the top right-hand panel of Figure 4. However, sunward ionospheric flows are seen between the downward and upward FAC cells. Flows, observed at a time mid-DMSP pass at 01:09 hr UT, about dusk head toward the nightside, suggesting a complicated convection pattern on this side of the polar cap. The particle precipitation data skims the sunward side of the polar cap, but various features can be seen in the spectrograms. The equatorward edge of the main auroral oval is seen prior to ζ. A reversed dispersion signature is seen between ζ and η, but at lower energies than the previously observed signatures. θ marks the poleward edge of the main auroral oval near noon. The solar wind density remains high above 40 cm^{-3}.

For the F16 Pass 44700, the auroral emissions are observed, but only in the LBHl band, pushed far into the dusk sector, as presented in Figure 5. The IMF B_Y component is at its largest for the time period presented, at around 40 nT. These emissions are colocated at the edge of the large upward NBZ FAC cell that extends from before just prior to noon until dusk. The downward NBZ FAC cell is indistinguishable from the weak Region 1 distribution of FAC at lower latitudes, as shown by the dominance of the upward polar cap NBZ FAC current magnitude trace in Figure 1e. Ionospheric flows, observed at a time mid-DMSP pass at 02:51 hr UT, that are located at the equatorward edge of the auroral emissions flow sunward on the dayside, in the postnoon sector. The satellite track clips the equatorward edge of the main auroral oval, and the particle precipitation data do not present any remarkable features. The solar wind density at this time remains elevated above nominal values but has dropped considerably from the large peak seen during previous passes to approximately 20 cm^{-3}. In Figure 1c, we see the start of a prolonged bay in the AL index. This bay may be associated with a tail reconnection during IMF-northward non-substorm event (TRINNI) (Grocott et al., 2003, 2004), as shown by the suggestion of a nightside auroral bulge seen in a previous DMSP/SSUSI image (not shown), although by this satellite pass, we barely sample the nightside portion of the polar cap. Strong westward ionospheric flows are, however, seen on the nightside in the premidnight sector, in the top right-hand plot of Figure 5.

The cusp spot emission remains near dusk for the remainder of the period when it is observable. The last observation of the cusp spot ends at 06:54 hr UT, when it is found at approximately 70°. This is consistent with the turn to southward IMF after 04:50 hr UT, and the IMF remains southward after this time, albeit under strong IMF B_Y positive conditions. The southward turning of the IMF would imply the commencement of low-latitude dayside reconnection, under the Expanding/Contracting Polar Cap model (Milan et al., 2012). By the end of the time period of Figure 1, the solar wind density is high, still around 20 cm^{-3}, although these densities are much reduced from those observed previously in the sequence. The upward NBZ FAC cell remains dominant and in the dusk sector. The AL index, in Figure 1c post 4 hr UT, shows several negative bays, indicative of a series of substorms. Beyond this time period, there are no auroral emissions in the polar cap that are discernible located poleward of the main auroral oval.

4. Discussion

We have presented a sequence of images of auroral emissions with accompanying simultaneous maps of FACs, ionospheric convection, and in situ particle precipitation data, which has tracked the appearance and movement of a high-latitude cusp spot inside the Northern Hemisphere polar cap auroral oval during a period of unusual and remarkable solar wind conditions. This cusp spot is remarkable due to its long

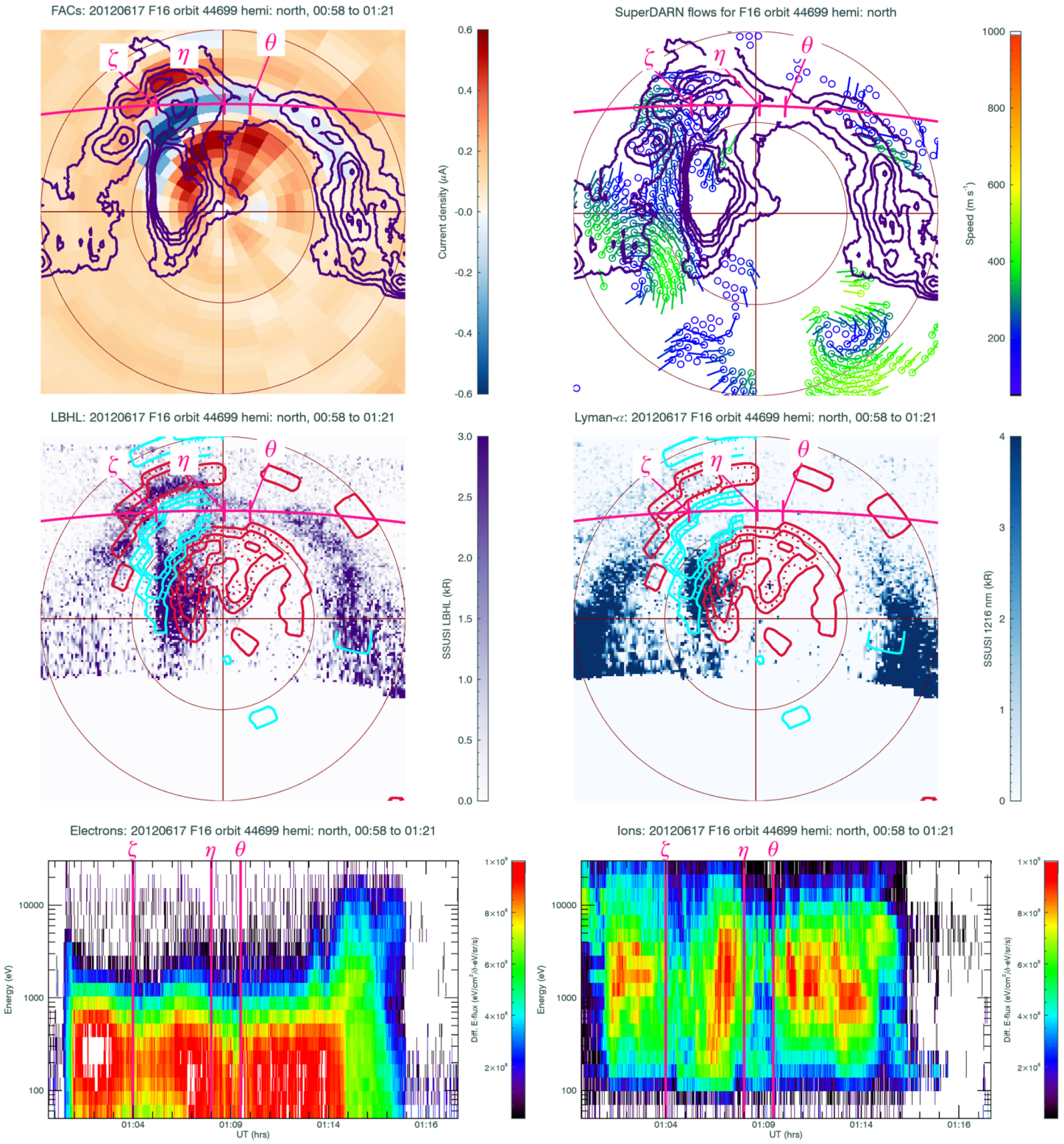

Figure 4. A selection of images relevant to DMSP F16 Orbit 44699. The format of the plots follows that of Figure 2.

duration, over approximately 11 hr, and its extreme displacement from the noon sector. The orientation of the IMF changes steadily over the interval, from northward B_Y dominated, which has allowed the extreme distortion of the convection cells, the NBZ FAC structure, and the location of the auroras to be studied.

The IMF and solar wind observations, especially with respect to the rotation in the IMF B_Y and B_Z components during the interval, suggest the passage of a magnetic cloud associated with an ICME. An ICME with magnetic cloud is listed for the interval in an online updated version of the catalog published by Richardson and Cane (2010). The cusp spot occurs during a period of high-magnitude IMF, which is primarily northward throughout the interval. Both the movement of the auroral cusp spot and the distribution of the NBZ FACs are consistent with the changes in the orientation of the IMF B_Y component, following the behavior of ionospheric convection under varying IMF as described by Cowley (2000). Phan et al. (2003) have previously observed cusp spot proton emission, associated with an ICME, but under lower solar wind dynamic pressure conditions. The proton cusp spot in this case lasted approximately 5.5 hr. The role of solar wind dynamic pressure in controlling the nature of the cusp spot proton-excited Lyman-α emission has been demonstrated by Frey et al. (2002). Recently, Østgaard et al. (2018) presented a case where a cusp spot was observed at an extremely distorted MLT position in electron-induced auroral emissions but was undetected via proton emissions. This cusp spot occurred around 17 hr MLT under large and positive IMF B_Y conditions and was found slightly duskward of a region of upward FAC as determined by the CHAMP spacecraft. The CHAMP spacecraft made localized measurements of FACs and was, therefore, not able to observe global patterns of NBZ currents such as those obtained by AMPERE. Østgaard et al. (2018) presented their cusp spot as a case of HiLDA emission. We dispute this, however, and attribute the observed emission to direct precipitation along open field lines under a scenario of lobe reconnection occurring at the high-latitude magnetopause under northwards IMF conditions, rather than HiLDAs, which are colocated with the upward NBZ FAC cell (Carter et al., 2018). The absence of proton-induced emission in the Østgaard et al. (2018) case may be due to lower observed solar wind proton densities, at around 20 cm^{-3}, compared to the higher densities, up to ~60 cm^{-3} seen at the beginning of this interval. In this case, when the densities have dropped to approximately 20 cm^{-3} during F16 Orbit Pass 44700, electron-induced auroral emission remains observable, whereas proton-induced emission does not. The cusp spot presented in this case in this paper shows how cusp spots at extreme MLTs can develop by tracking the cusp spot under a changing IMF orientation with respect to the NBZ FAC pattern.

Cusp spot auroral emissions are observed in the polar cap and are seen at the eastern side of the upward NBZ FAC cell, or straddling the spatial region between the upward and downward NBZ FAC cells. The NBZ FACs during this interval cover a large spatial area of the polar cap and show total current magnitudes that are more often seen for the Regions 1 and 2 current systems (Coxon et al., 2014, 2016). Peak magnitudes of the current densities in the limited dayside high-latitude region inside of 12° colatitude reached 4.2 $\mu A\ m^{-2}$ for the upward current and $-5.7\ \mu A\ m^{-2}$ for the downward current. Peak magnitudes in NBZ current reached 0.13 MA (which occurred at 11° colatitude and 11 hr MLT) and −0.06 MA (which occurred at 8° colatitude and 17 hr MLT) for upward and downward currents, respectively, assuming a height of 110 km. These values are comparable to those seen by Araki et al. (1984), who also showed that the NBZ currents exhibited larger current densities than those of Region 1. The NBZ FACs respond as expected, with the orientation of the IMF B_Y component, so that under highly positive IMF B_Y conditions, the upward cell moves toward noon. The movement of the NBZ cells, with respect to the prevailing IMF conditions, has been shown on a statistical basis in Carter et al. (2017) and Carter et al. (2018). There is no time delay suggested between changes in the distribution of the upward and downward NBZ FAC cell, under large variations in direction of the IMF B_Y component, and those of the auroral emissions. The dayside polar cap responds quickly to changes in the magnitude and orientation of the IMF. The fast response of the polar cap FACs to changes in IMF orientation was recently demonstrated by Taguchi et al. (2015) during a transition from a IMF B_Z-dominated to IMF B_Y-dominated scenario in approximately 10 min, and again by Coxon et al. (2019) following a statistical study of FACs, which also showed a 10-min response at high latitude. The IMF turns briefly southward twice after 20 hr UT on 16 June 2012 and each time for 4 min in duration. Lockwood et al. (2003) observed a brightening of Lyman-α emission associated with a cusp spot during a southward turning of the IMF, which also moved the cusp spot equatorward. The southward turnings in this study last for a much shorter duration than the expected propagation time of the solar wind through the magnetosheath, of approximately 8 min. In addition, the cadence of SSUSI images does not allow us to follow any slight equatorward shift of the cusp spot during these brief incursions to southward IMF, unlike the fast 2-min resolution used by Lockwood et al. (2003), and we do not see any short-term brightening of the cusp spot auroral emissions associated with the southward turnings at these times.

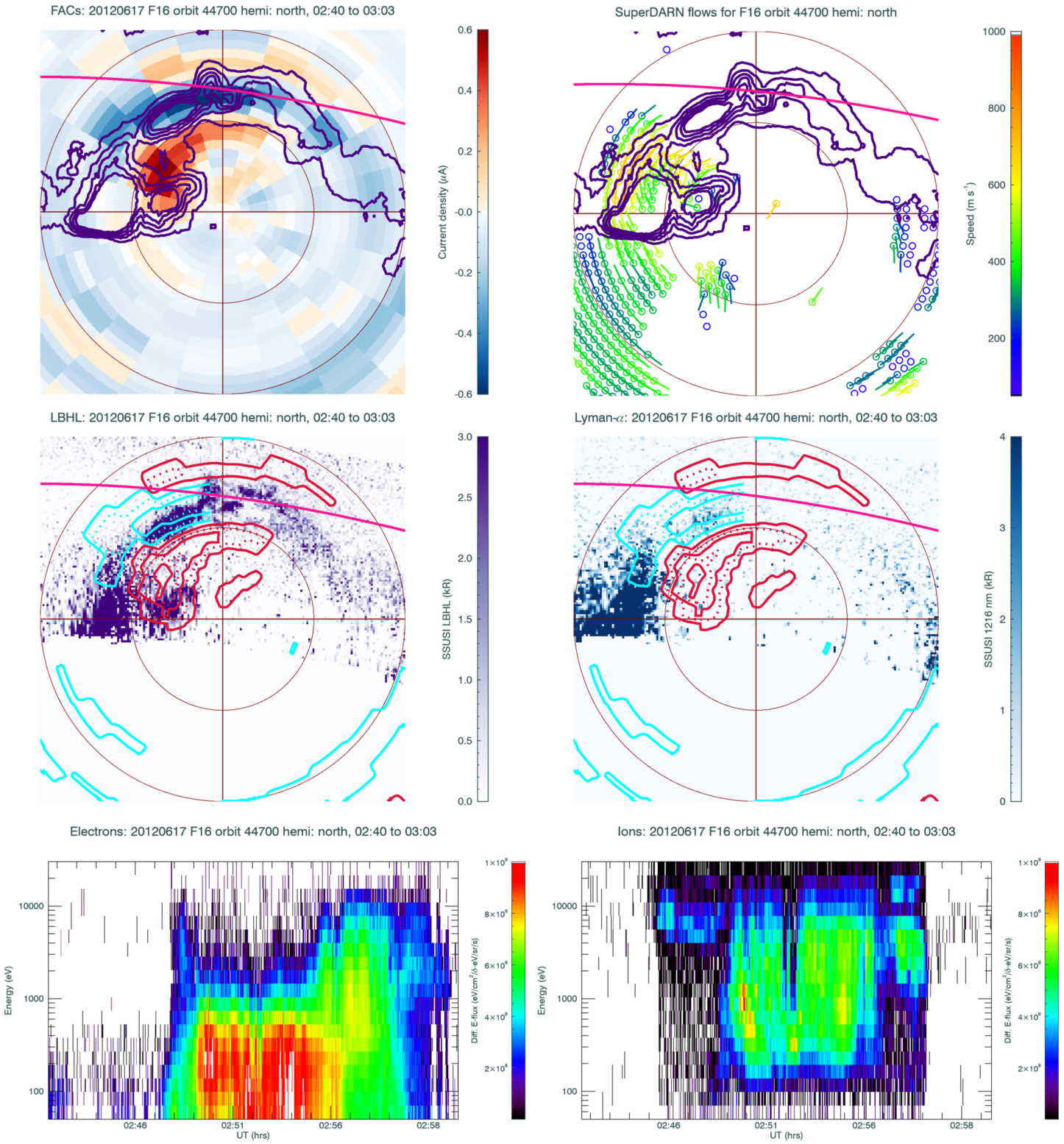

Figure 5. A selection of images relevant to DMSP F16 Orbit 44700. The format of the plots follows that of Figure 2.

We do not observe LBHl emissions that are colocated with the upward NBZ FAC cell, or HiLDAs (Frey, 2007; Korth et al., 2014, and references therein). It has been demonstrated that HiLDAs are seen in the summer hemisphere (Carter et al., 2018; Frey et al., 2004), in the LBHl band, resulting primarily from electron

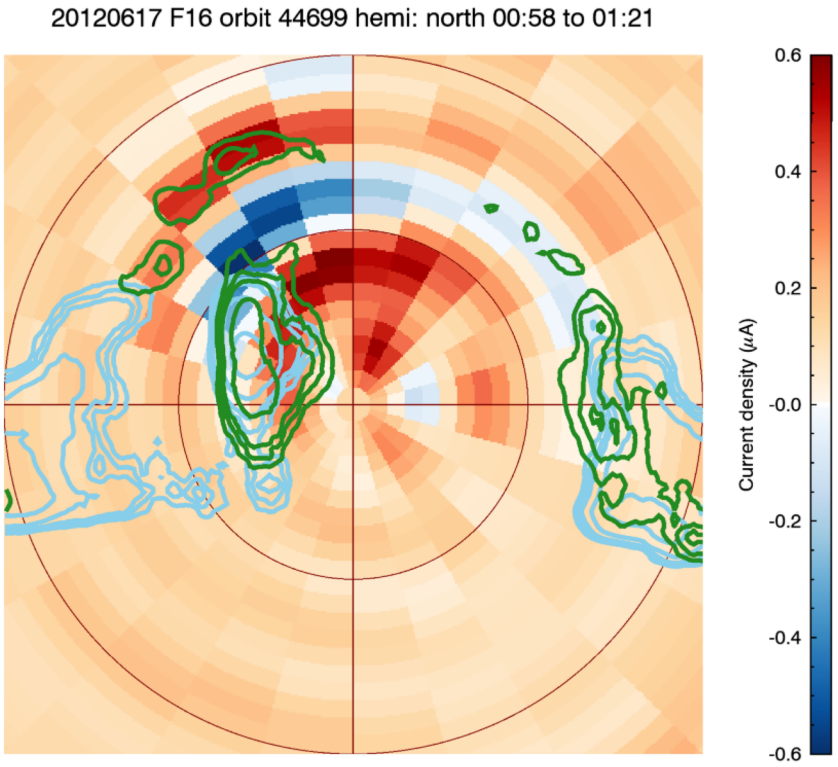

Figure 6. FACs image, with upward currents in red and downward currents in blue, with contours for LBHl (green) and Lyman-α (sky blue) emission, during one particular satellite pass. Contours are plotted at 1.6, 2.2, 2.8, 5.0, and 10 kR.

precipitation, rather than in the Lyman-α band, that results from precipitating protons. It has been suggested that these HiLDAs are controlled by solar wind speed, rather than solar wind density, occurring when the solar wind density is below 4 cm^{-3} (Frey et al., 2004), although the mechanism for this limitation has not been established. The interval here exhibits very high densities, at times reaching 60 cm^{-3}. We illustrate that we are observing cusp spot, rather than HiLDA emission, by plotting both LBHl and Lyman-α contours on a single image of FACs in Figure 6. The FAC image is taken from AMPERE data obtained in the 2-min interval around 01:10 hr UT. We only plot contours for the brightest emissions. Both LBHl and Lyman-α are spatially colocated, and the brightest emission contours occur in the narrow region between the downward and upward FAC NBZ cells.

We attribute the auroral emissions observed, in both the LBHl and Lyman-α bands, to direct precipitation under lobe reconnection at the high-latitude magnetopause, forming a cusp spot in the high-latitude polar cap. This cusp spot moves gradually into the high-latitude polar cap, extending beyond the dawn-dusk meridian (e.g., Figure 6), as lobe connection continues under the prolonged northward IMF conditions, mapping increasingly antisunward into the lobes of the magnetosphere. We illustrate this scenario in Figure 7 for the dayside polar cap, where the Sun is toward the top of the image and the open/closed field line boundary is represented by the green semicircle. Figure 7a is for IMF $B_Y \simeq 0$ nT, and Figure 7b is for IMF $B_Y > 0$ nT conditions. The antisunward extension of the spot occurs as magnetic tension forces on newly reconnected lobe field lines initially pulls them sunward, such that the reconnection X-line maps to higher latitudes than the dayside open/closed field line boundary. Particle precipitation, resulting in dispersed signatures in the case of ions, and auroral emission occur on these newly reconnected field lines downstream, that is, sunward, of the reconnection X line. Hence, we place the X line at the most antisunward edge of the emission, as seen in Figure 7a or 7b. The cusp spot or ion dispersion is shown by the purple shaded areas in the figure, with the gradient showing the sense of dispersion from high to low energy. If the reconnection rate exceeds the rate at which the field lines are convected sunward and then azimuthally, the X line will progress antisunward. The cusp spot location in Figure 7 is different to that of the HiLDA emission as shown in Figure 5 of Carter et al.

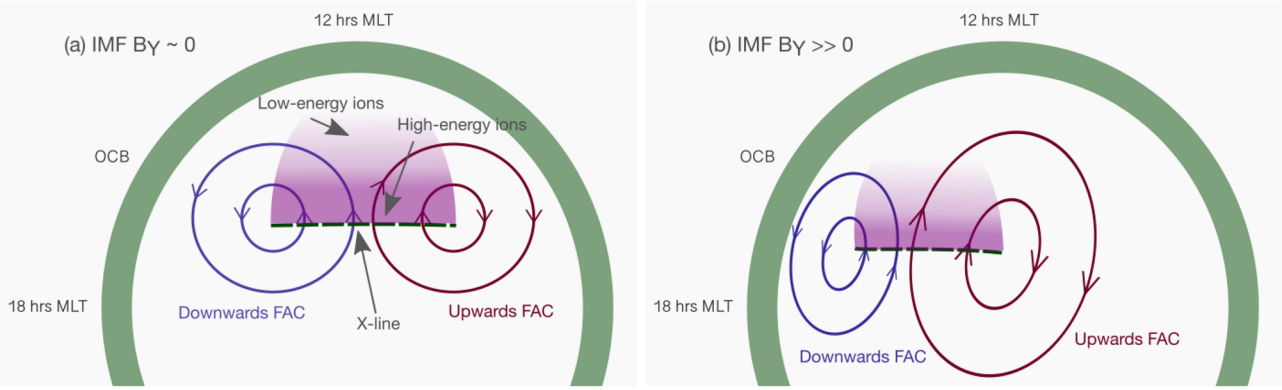

Figure 7. Schematic of the polar cap under extremely northward IMF conditions, for (a) $B_Y \simeq 0$ nT and (b) $B_Y \gg 0$ nT. Noon is to the top and dusk to the left. The dayside portion of the open/closed field line boundary is shown in green. The footprint of the lobe reconnection X line is shown by the dashed green line. The shaded purple areas show regions of aurora and dispersion ions, sunward of the X lines. Two sunward convection cells are drawn inside the polar cap. The dawn cell, shown in red, is associated with upward FAC, and the dusk cell, shown in blue, with downward FAC.

(2018), which is illustrated to be colocated with the upward FAC cell inside the polar cap. The difference in location reflects the difference in mechanism between the two phenomena.

The solar wind density is extremely high throughout this interval, implying that there are sufficient numbers of particles to cause detectable auroral emissions in both the LBHl and Lyman-α bands. The Lyman-α (proton) emission becomes undetectable from 02:40 hr UT, before that of the LBHl (mainly electron) emissions. The dayside polar cap LBHl emissions show marked increases in mean radiance (empty purple rectangles, Figure 1f), as opposed to the total polar cap radiances (filled purple rectangles). In contrast, the dayside polar cap Lyman-α emissions (empty blue rectangles) dominate the total polar cap mean radiances when very high density pulses (>40 cm^{-3}) are observed in the solar wind, indicating that an increase in total number of precipitating particles is required to make the Lyman-α emissions (protons) observable by the SSUSI cameras. This is consistent with the statement of Bryant et al. (2013) that higher quantities of precipitating particles lead to brighter auroral emissions in polar cap spots. We interpret the auroral spot as occurring on open field lines following high-latitude reconnection. After the IMF has turned southward at 04:50 hr UT on 17 June 2012, the cusp spot is still visible in the LBHl emissions for approximately 2.5 hr, but it is no longer seen beyond 07 hr UT. This may indicate that high-latitude lobe reconnection is still possible during this time under such IMF B_Y-dominated conditions and the extremely distorted cusp spot, ionospheric flows, and NBZ current distribution reflect the persistence of this phenomenon beyond the southward turning of the IMF. The cusp spot will then persist until the IMF B_Y component reduces, or when precipitating particles associated with the reconnected field lines have drained into the polar cap and the spot becomes subvisual.

Several passes of the DMSP satellites bisect the region of brightest cusp spot emission, and we observe a colocated reverse ion-dispersion signature with this emission in the spectrograms of Figures 2–5. In some satellite passes, the dispersion signature may occur twice. Ion dispersion signatures are well-established indicators of high-latitude lobe reconnection (Burch et al., 1980; Chisham et al., 2004). There is debate in the community regarding the nature of patchy reconnection signatures, and cusp spots provide one observable to study this phenomenon. However, the time resolution of the DMSP/SSUSI data per polar cap traversal does not allow for such an investigation here.

We support the auroral emission and FAC data with ionospheric convection flows, as obtained by SuperDARN. The flows are often sparse, but those that appear are more prevalent on the dayside. The flows are associated with the eastern edge of the area of brightest auroral emissions, initially moving sunward and then rotating toward either dawnward or duskward. The flows are strongest in the channel between the two NBZ cells. The dusk cell is more often seen in the data, for example, Orbit 13727 in Figure 2. Later in the interval, flows appear on the nightside, coincident with the appearance of an increased nightside auroral bulge.

At the end of the interval, the main auroral oval expands to lower latitudes under southward IMF conditions, and some nighttime auroral bulge activity is seen in the later nightside, as low-latitude dayside reconnection begins, eroding the dayside magnetopause and adding flux to the polar cap (Milan et al., 2012). This coincides with the end of the interval and the disappearance of the cusp spot auroral emissions.

5. Conclusions

We have presented an interval when spatially large NBZ FACs that dominated the main Regions 1 and 2 FAC systems were seen inside the polar cap over an 11-hr period. Simultaneously with the appearance of these currents were observations of both electron and proton precipitation, which resulted in an auroral cusp spot. This cusp spot extended from the east side of the upward NBZ cell to the western flank of the downward NBZ cell in the sunward flow region. The study of cusp spots in the ionosphere provides a method to remotely investigate reconnection sites at the more distant magnetopause. Peaks in auroral emissions are associated with pulses in solar wind density. Ionospheric convection in the dayside polar cap, particularly on the dusk and evening side of the polar cap, showed flows in a direction compatible with convection cells associated with lobe reconnection. The cusp spot and associated high-latitude FACs both changed location under the influence of the large and mainly positive IMF B_Y component yet during sustained northward IMF B_Z positive conditions, which extremely distorted the polar cap features from a nominal $B_Y = 0$ nT distribution. The long duration of the cusp spot and presence of NBZ FAC cells and their movement, along with the observed cusp dispersion signatures, is compatible with a model of sustained reconnection at the high-latitude magnetopause in the lobe regions occurring at increasing tailward locations as the IMF northward conditions persist under a changing B_Y orientation. The interval is truncated by a southward turning of the IMF and subsequence dayside driving of the magnetopause and expansion of the polar cap.

Data Availability Statement

The DMSP/SSUSI file type EDR-AUR data were obtained from http://ssusi.jhuapl.edu (data Version 0106, software Version 7.0.0, and calibration period Version E0018). AMPERE data were obtained online (from http://ampere.jhuapl.edu). Solar wind data were obtained from the NASA/GSFC OMNI facility (http://omniweb.gsfc.nasa.gov) and included the geomagnetic and auroral indices SYM-H, AU, and AL as provided by the WDC for Geomagnetism, Kyoto (http://wdc.kugi.kyoto-u.ac.jp/wdc/Sec3.html). The ICME list used is found online (at http://www.srl.caltech.edu/ACE/ASC/DATA/level3/icmetable2.htm). The authors acknowledge the use of SuperDARN data. SuperDARN is a collection of radars funded by national scientific funding agencies of Australia, Canada, China, France, Japan, South Africa, United Kingdom, and United States of America. SuperDARN data can be found online (at https://www.bas.ac.uk/project/superdarn/#data).

Acknowledgments

J. A. C., S. E. M., and M. L. gratefully acknowledge support from the Science Technology Facilities Council (STFC) Consolidated Grant ST/S000429/1. A. R. F. and H. S. are supported by STFC studentships. This research used the ALICE and SPECTRE High Performance Computing Facility at the University of Leicester.

References

Anderson, B. J., Takahashi, K., & Toth, B. A. (2000). Sensing global Birkeland currents with iridium® engineering magnetometer data. *Geophysical Research Letters*, *27*, 4045–4048. https://doi.org/10.1029/2000GL000094

Araki, T., Kamei, T., & Iyemori, T. (1984). Polar cap vertical currents associated with northward interplanetary magnetic field. *Geophysical Research Letters*, *11*(1), 23–26. https://doi.org/10.1029/GL011i001p00023

Bryant, C. R., McWilliams, K. A., & Frey, H. U. (2013). Localized dayside proton aurora at high latitudes. *Journal of Geophysical Research: Space Physics*, *118*, 3157–3164. https://doi.org/10.1002/jgra.50311

Burch, J. L., Reiff, P. H., Spiro, R. W., Heelis, R. A., & Fields, S. A. (1980). Cusp region particle precipitation and ion convection for northward interplanetary magnetic field. *Geophysical Research Letters*, *7*(5), 393–396. https://doi.org/10.1029/GL007i005p00393

Carter, J. A., Milan, S. E., Fear, R. C., Walach, M.-T., Harrison, Z. A., Paxton, L. J., & Hubert, B. (2017). Transpolar arcs observed simultaneously in both hemispheres. *Journal of Geophysical Research: Space Physics*, *122*, 6107–6120. https://doi.org/10.1002/2016JA023830

Carter, J. A., Milan, S. E., Fogg, A. R., Paxton, L. J., & Anderson, B. J. (2018). The association of high-latitude dayside aurora with NBZ field-aligned currents. *Journal of Geophysical Research: Space Physics*, *123*, 3637–3645. https://doi.org/10.1029/2017JA025082

Chisham, G., Freeman, M. P., Coleman, I. J., Pinnock, M., Hairston, M. R., Lester, M., & Sofko, G. (2004). Measuring the dayside reconnection rate during an interval of due northward interplanetary magnetic field. *Annales Geophysicae*, *22*(12), 4243–4258. https://doi.org/10.5194/angeo-22-4243-2004

Chisham, G., Lester, M., Milan, S. E., Freeman, M. P., Bristow, W. A., Grocott, A., et al. (2007). A decade of the Super Dual Auroral Radar Network (SuperDARN): Scientific achievements, new techniques and future directions. *Surveys in Geophysics*, *28*, 33–109. https://doi.org/10.1007/s10712-007-9017-8

Clausen, L. B. N., Baker, J. B. H., Ruohoniemi, J. M., Milan, S. E., & Anderson, B. J. (2012). Dynamics of the Region 1 Birkeland current oval derived from the Active Magnetosphere and Planetary Electrodynamics Response Experiment (AMPERE). *Journal of Geophysical Research*, *117*, A06233. https://doi.org/10.1029/2012JA017666

Cowley, S. W. H. (2000). TUTORIAL: Magnetosphere-ionosphere interactions: A tutorial review. *Washington DC American Geophysical Union Geophysical Monograph Series*, *118*, 91. https://doi.org/10.1029/GM118p0091

Coxon, J. C., Milan, S. E., Carter, J. A., Clausen, L. B. N., Anderson, B. J., & Korth, H. (2016). Seasonal and diurnal variations in AMPERE observations of the Birkeland currents compared to modeled results. *Journal of Geophysical Research: Space Physics*, *121*, 4027–4040. https://doi.org/10.1002/2015JA022050

Coxon, J. C., Milan, S. E., Clausen, L. B. N., Anderson, B. J., & Korth, H. (2014). The magnitudes of the Regions 1 and 2 Birkeland currents observed by AMPERE and their role in solar wind-magnetosphere-ionosphere coupling. *Journal of Geophysical Research: Space Physics*, *119*, 9804–9815. https://doi.org/10.1002/2014JA020138

Coxon, J. C., Shore, R. M., Freeman, M. P., Fear, R. C., Browett, S. D., Smith, A. W., et al. (2019). Timescales of Birkeland currents driven by the IMF. *Geophysical Research Letters*, *46*, 7893–7901. https://doi.org/10.1029/2018GL081658

Escoubet, C. P., Berchem, J., Trattner, K. J., Pitout, F., Richard, R., Taylor, M. G. G. T., et al. (2013). Double cusp encounter by Cluster: Double cusp or motion of the cusp? *Annales Geophysicae*, *31*, 713–723. https://doi.org/10.5194/angeo-31-713-2013

Fogg, A. R., Lester, M., Yeoman, T. K., Burrell, A. G., Imber, S. M., Milan, S. E., et al. (2020). An improved estimation of SuperDARN Heppner-Maynard boundaries using AMPERE data. *Journal of Geophysical Research: Space Physics*, *125*, e2019JA027218. https://doi.org/10.1029/2019JA027218

Frey, H. U. (2007). Localized aurora beyond the auroral oval. *Reviews of Geophysics*, *45*, RG1003. https://doi.org/10.1029/2005RG000174

Frey, H. U., Immel, T. J., Lu, G., Bonnell, J., Fuselier, S. A., Mende, S. B., et al. (2003). Properties of localized, high latitude, dayside aurora. *Journal of Geophysical Research*, *108*(A4), 8008. https://doi.org/10.1029/2002JA009332

Frey, H. U., Mende, S. B., Immel, T. J., Fuselier, S. A., Claflin, E. S., Gérard, J.-C., & Hubert, B. (2002). Proton aurora in the cusp. *Journal of Geophysical Research*, *107*, 1091. https://doi.org/10.1029/2001JA900161

Frey, H. U., Østgaard, N., Immel, T. J., Korth, H., & Mende, S. B. (2004). Seasonal dependence of localized, high-latitude dayside aurora (HiLDA). *Journal of Geophysical Research*, *109*, A04303. https://doi.org/10.1029/2003JA010293

Fuselier, S. A., Mende, S. B., Moore, T. E., Frey, H. U., Petrinec, S. M., Claflin, E. S., & Collier, M. R. (2003). Cusp dynamics and ionospheric outflow. *Space Science Reviews*, *109*, 285–312. https://doi.org/10.1023/B:SPAC.0000007522.71147.b3

Greenwald, R. A., Baker, K. B., Dudeney, J. R., Pinnock, M., Jones, T. B., Thomas, E. C., et al. (1995). Darn/Superdarn: A global view of the dynamics of high-latitude convection. *Space Science Reviews*, *71*, 761–796. https://doi.org/10.1007/BF00751350

Grocott, A., Badman, S., Cowley, S., Yeoman, T., & Cripps, P. (2004). The influence of IMF By on the nature of the nightside high-latitude ionospheric flow during intervals of positive IMF Bz. *Annales Geophysicae*, *22*, 1755–1764. https://doi.org/10.5194/angeo-22-1755-2004

Grocott, A., Cowley, S. W. H., & Sigwarth, J. B. (2003). Ionospheric flow during extended intervals of northward but B_y -dominated IMF. *Annales Geophysicae*, *21*, 509–538. https://doi.org/10.5194/angeo-21-509-2003

Iijima, T., Potemra, T. A., Zanetti, L. J., & Bythrow, P. F. (1984). Large-scale Birkeland currents in the dayside polar region during strongly northward IMF: A new Birkeland current system. *Journal of Geophysical Research*, *89*(A9), 7441–7452. https://doi.org/10.1029/JA089iA09p07441

King, J. H., & Papitashvili, N. E. (2005). Solar wind spatial scales in and comparisons of hourly Wind and ACE plasma and magnetic field data. *Journal of Geophysical Research*, *110*, A02104. https://doi.org/10.1029/2004JA010649

Korth, H., Anderson, B. J., Frey, H. U., & Waters, C. L. (2005). High-latitude electromagnetic and particle energy flux during an event with sustained strongly northward IMF. *Annales Geophysicae*, *23*, 1295–1310. https://doi.org/10.5194/angeo-23-1295-2005

Korth, H., Zhang, Y., Anderson, B. J., Sotirelis, T., & Waters, C. L. (2014). Statistical relationship between large-scale upward field-aligned currents and electron precipitation. *Journal of Geophysical Research: Space Physics*, *119*, 6715–6731. https://doi.org/10.1002/2014JA019961

Liou, K., Zhang, Y.-L., Newell, P. T., Paxton, L. J., & Carbary, J. F. (2011). TIMED/GUVI observation of solar illumination effect on auroral energy deposition. *Journal of Geophysical Research*, *116*, A09305. https://doi.org/10.1029/2010JA016402

Lockwood, M., Lanchester, B. S., Frey, H. U., Throp, K., Morley, S. K., Milan, S. E., & Lester, M. (2003). IMF control of cusp proton emission intensity and dayside convection: Implications for component and anti-parallel reconnection. *Annales Geophysicae*, *21*, 955–982. https://doi.org/10.5194/angeo-21-955-2003

Milan, S. E., Gosling, J. S., & Hubert, B. (2012). Relationship between interplanetary parameters and the magnetopause reconnection rate quantified from observations of the expanding polar cap. *Journal of Geophysical Research*, *117*, A03226. https://doi.org/10.1029/2011JA017082

Milan, S. E., Lester, M., Cowley, S. W. H., & Brittnacher, M. (2000). Dayside convection and auroral morphology during an interval of northward interplanetary magnetic field. *Annales Geophysicae*, *18*(4), 436–444. https://doi.org/10.1007/s00585-000-0436-9

Nishitani, N., Ruohoniemi, J. M., Lester, M., Baker, J. B. H., Koustov, A. V., Shepherd, S. G., et al. (2019). Review of the accomplishments of mid-latitude super dual auroral radar network (SuperDARN) hF radars. *Progress in Earth and Planetary Science*, *6*(1), 27.

Østgaard, N., Reistad, J. P., Tenfjord, P., Laundal, K. M., Rexer, T., Haaland, S. E., et al. (2018). The asymmetric geospace as displayed during the geomagnetic storm on August 17, 2001. In *EGU General Assembly Conference Abstracts*, pp. 2553.

Paxton, L. J., Meng, C.-I., Fountain, G. H., Ogorzalek, B. S., Darlington, E. H., Gary, S. A., et al. (1992). Special Sensor Ultraviolet Spectrographic Imager (SSUSI)—An instrument description. In *Instrumentation for Planetary and Terrestrial Atmospheric Remote Sensing* (S. Chakrabarti, & A. B. Christensen, Eds.), *1745*, pp. 2–15. https://doi.org/10.1117/12.60595

Paxton, L. J., Schaefer, R. K., Zhang, Y., & Kil, H. (2017). Far ultraviolet instrument technology. *Journal of Geophysical Research: Space Physics*, *122*, 2706–2733. https://doi.org/10.1002/2016JA023578

Paxton, L. J., Schaefer, R. K., Zhang, Y., Kil, H., & Hicks, J. E. (2018). SSUSI and SSUSI-Lite: Providing space situational awareness and support for over 25 years. *JOHNS HOPKINS APL TECHNICAL DIGEST*, *34*(3), 388–400.

Paxton, L. J., & Zhang, Y. (2016). *Far ultraviolet imaging of the aurora. In Space Weather Fundamentals*: CRC press.

Phan, T., Frey, H. U., Frey, S., Peticolas, L., Fuselier, S., Carlson, C., et al. (2003). Simultaneous cluster and IMAGE observations of cusp reconnection and auroral proton spot for northward IMF. *Geophysical Research Letters*, *30*(10), 1509. https://doi.org/10.1029/2003GL016885

Redmon, R. J., Denig, W. F., Kilcommons, L. M., & Knipp, D. J. (2017). New DMSP database of precipitating auroral electrons and ions. *Journal of Geophysical Research: Space Physics*, *122*, 9056–9067. https://doi.org/10.1002/2016JA023339

Richardson, I. G., & Cane, H. V. (2010). Near-Earth interplanetary coronal mass ejections during Solar Cycle 23 (1996–2009): Catalog and summary of properties. *Solar Physics*, *264*(1), 189–237. https://doi.org/10.1007/s11207-010-9568-6

Ruohoniemi, J. M., & Baker, K. B. (1998). Large-scale imaging of high-latitude convection with Super Dual Auroral Radar Network HF radar observations. *Journal of Geophysical Research*, *103*, 20,797–20,811. https://doi.org/10.1029/98JA01288

Sandholt, P. E., Farrugia, C. J., Moen, J. A. B., Noraberg, O., Lybekk, B. A. B., Sten, T., & Hansen, T. (1998). A classification of dayside auroral forms and activities as a function of interplanetary magnetic field orientation. *Journal of Geophysical Research*, *103*(A10), 23,325–23,345. https://doi.org/10.1029/98JA02156

Shue, J.-H., & Song, P. (2002). The location and shape of the magnetopause. *Planetary and Space Science*, *50*, 549–558. https://doi.org/10.1016/S0032-0633(02)00034-X

Strickland, D. J., Evans, J. S., & Paxton, L. J. (1995). Satellite remote sensing of thermospheric O/N2 and solar EUV. 1: Theory. *Journal of Geophysical Research*, *100*, 12. https://doi.org/10.1029/95JA00574

Strickland, D. J., Lean, J. L., Meier, R. R., Christensen, A. B., Paxton, L. J., Morrison, D., et al. (2004). Solar EUV irradiance variability derived from terrestrial far ultraviolet dayglow observations. *Geophysical Research Letters*, *31*, L03801. https://doi.org/10.1029/2003GL018415

SuperDARN Data Analysis Working Group, Thomas, E. G., Ponomarenko, P. V., Billett, D. D., Bland, E. C., Burrell, A. G., et al. (2018). SuperDARN Radar Software Toolkit (RST) 4.2. https://doi.org/10.5281/zenodo.1403226

Taguchi, S., Tawara, A., Hairston, M. R., Slavin, J. A., Le, G., Matzka, J., & Stolle, C. (2015). Response of reverse convection to fast IMF transitions. *Journal of Geophysical Research: Space Physics*, *120*, 4020–4037. https://doi.org/10.1002/2015JA021002

Vennerstrøm, S., Moretto, T., Olsen, N., Friis-Christensen, E., Stampe, A. M., & Watermann, J. F. (2002). Field-aligned currents in the dayside cusp and polar cap region during northward IMF. *Journal of Geophysical Research*, *107*(A8), SMP 18–1–SMP 18–5. https://doi.org/10.1029/2001JA009162

Waters, C. L., Anderson, B. J., & Liou, K. (2001). Estimation of global field aligned currents using the iridium® system magnetometer data. *Geophysical Research Letters*, *28*, 2165–2168. https://doi.org/10.1029/2000GL012725

Zhang, Y., & Paxton, L. J. (2008). An empirical Kp-dependent global auroral model based on TIMED/GUVI FUV data. *Journal of Atmospheric and Solar-Terrestrial Physics*, *70*, 1231–1242. https://doi.org/10.1016/j.jastp.2008.03.008